ORIGINAL CONTRIBUTION

FFEMS Fatigue & Fracture of Engineering Materials & Structures   WILEY

Experimental and numerical evaluations on the effects of adhesive fillet, overlap length and unbonded area in adhesive-bonded joints

Guanghan Wu[1] | Dayong Li[1] | Wei-Jen Lai[2] | Qiuren Chen[3] |
Yandong Shi[4] | Li Huang[4] | Shiyao Huang[2] | Hongtae Kang[3] |
Yinghong Peng[1] | Xuming Su[2]

[1]State Key Laboratory of Mechanical Systems and Vibration, Shanghai Jiao Tong University, Shanghai, 200240, China

[2]Ford Motor Company, Research and Innovation Center, Dearborn, MI, 48121, USA

[3]College of Engineering and Computer Science, University of Michigan-Dearborn, Dearborn, MI, 48128, USA

[4]Materials and Process Research, Ford Motor Research and Engineering Center, Nanjing, 211100, China

Correspondence
Dayong Li, State Key Laboratory of Mechanical Systems and Vibration, Shanghai Jiao Tong University, Shanghai 200240, China.
Email: dyli@sjtu.edu.cn

Abstract

To realize robust structural design, the effects of the adhesive fillet, overlap length and unbonded area in adhesive-bonded joints need to be fully understood and incorporated into a fatigue life estimation method. In the present work, both static and fatigue experiments are performed on six types of adhesive-bonded joints to illuminate these effects systematically. A straightforward total fatigue life evaluation method is proposed to address these effects. A statistical crack initiation model is established based on the fatigue data of bulk adhesive specimens. Growth life is calculated using the interfacial crack model and mixed mode crack growth method. Good correlation is observed between the calculated and experimental fatigue lives. Furthermore, the effects of the adhesive fillet, overlap length and unbonded area are analysed based on both calculated and experimental results. Results indicate that adhesive fillet postpones crack initiation by reducing local strain level, both overlap length and unbonded area change the growth life by length. Besides, overlap length promotes the fraction of mode II strain energy release rate in total, reducing crack growth rates and extending growth life.

KEYWORDS

adhesive fillet, crack initiation, local strain-stress approach, mixed mode crack growth, overlap length, unbonded area

1 | INTRODUCTION

The outstanding mechanical properties of adhesive-bonded joints, for example, lightweight, uniform stress distribution, watertight, excellent corrosion protection,[1] enhanced noise, vibration and harshness (NVH) performance,[2] and the ability to join different materials,[3,4] lead to increasing use in joining complex auto body structures.[5] From the durability design's perspective,[6] there is a specific need for analysis and design tools that can provide physical insight and characterize the effects of design variables.

Regarding the adhesive-bonded joints, the adhesive fillet, overlap length and unbonded area are the most widely used design variables which could significantly change the joint's durability performance.[7,8] Among the whole fatigue failure process, adhesive fillets have been identified as most contributing to extend crack initiation by reducing stress concentration at the interface corner between substrate and adhesive. By recording the back-face strain

during tests and measuring the damage in different locations of adhesive-bonded joints, Solana and Crocombe[9] found that the damage in adhesive-bonded joints appeared first in the fillet. Removing the adhesive fillet will eliminate the initiation phase and consequently reduce the fatigue life.[10] Furthermore, the proportion of crack initiation life in total life has been found to vary in different types of specimens.[11,12] To establish crack initiation model, the intensity of the singular stress field[13,14] has been considered and transformed into the fatigue parameter[13,15] to correlate the test data. However, it is not widely used, especially for a cohesive failure crack. One of the possible reasons is that the stress singularity will be significantly changed by the round radius, which is created during the substrate cutting process.

Generally, the total fatigue failure of an adhesive-bonded joint consists of crack initiation[16,17] and subsequent crack growth.[18–21] It has been reported that the proportion of crack growth life will increase with increasing load levels.[22–24] At the same external load level, the fatigue life of joints with larger overlap length is longer than those with smaller ones, which can be attributed to longer crack growth length.[25] Jen and Ko[26] studied the effect of overlap length on the fatigue strength of epoxy adhesive-bonded aluminium single lap joints. Results indicate that fatigue resistance decreases with the decreasing overlap length. The unbonded area is expected to have a similar effect of overlap length. By comparing the fatigue behaviour of weld-bonded and adhesive-bonded joints,[27,28] Xu et al.[28] found that at the same external load level, the fatigue life of weld-bonded joints is smaller than that of adhesive-bonded joints, especially at higher load levels. They found the adhesive was not bonded at the weld nugget area due to the burning of adhesive during nugget formation. However, these effects have not been characterized by existing fatigue models.

Fracture mechanism-based methods are commonly used to predict crack growth life. The crack growth laws in mode I and mode II are widely determined by using double cantilever beam (DCB) specimens[18–20] and 3-points end-notched flexure (3ENF) specimens,[19] respectively. Crack growth life was calculated by integrating Paris law from an assumed initial crack to final failure. But the estimated results are not promising. One of the reasons is the complexity of loading conditions in adhesive-bonded joints. Most adhesives are under multiaxial stress conditions[21] in practice, for example, peel, shear and axial stresses in the adhesive layer, even for the simplest single lap joint,[29] which bring challenges to growth life estimation. Furthermore, the crack initiation phase was omitted in these research studies, which would lead to conservative predicted results.[30] By

assuming the crack growth of the adhesive as a result of progressive material deterioration in the cohesive zone and the interaction thereof with the surrounding continuum,[24,31] the cohesive damage model (CDM) was developed to simulate the entire failure process of adhesive-bonded joints. The location of crack initiation and growth is usually determined by utilizing a promising phenomenological criterion[32–34] based on the pure mode I and mode II values, which can be determined directly or inversely. Mesh sensitivity can also be avoided given an appropriate mesh refinement. But time-consuming computation is still inevitable due to the mesh refinement and sensitivity examination induced by stress singularity at the substrate edge.

In the present work, the effects of the adhesive fillet, overlap length and unbonded area are systematically illustrated in aluminium adhesive-bonded lap-shear joints. A total fatigue estimation method is proposed for the performance characterization by straightforwardly dividing the failure into crack initiation and growth. Crack initiation is modelled using the fatigue test data of bulk adhesive specimens fitted by the Manson-Coffin-Basquin equation. Local strain data obtained from detailed 3D finite element (FE) models are used for the crack initiation site and life predictions. Crack growth life is calculated through the integration of crack growth rates as a function of strain energy release rates. The interfacial crack model is coupled with mixed mode crack growth model to capture the effect of mixed mode ratio. Finally, calculated results are compared and analysed together with experimental results, well characterizing the effects of the adhesive fillet, overlap length and unbonded area.

2 | EXPERIMENTS

Both bulk adhesive specimens and adhesive-bonded joints are tested in this study. Fatigue test results of bulk adhesive specimens are used for crack initiation modelling. Quasi-static and fatigue tests on adhesive-bonded joints are used to illustrate the effects of adhesive fillet, overlap length and unbonded area on crack initiation and growth.

2.1 | Specimen preparation and test setup

The static and fatigue tests follow ISO 527-2[35] and ASTM D-3166-99[36] for bulk adhesive specimens and adhesive-bonded lap-shear joints, respectively. Figure 1 shows the specimen configurations and dimensions for both specimens, where L is the overlap length and D is the diameter of the embedded polytetrafluoroethylene (PTFE) tape
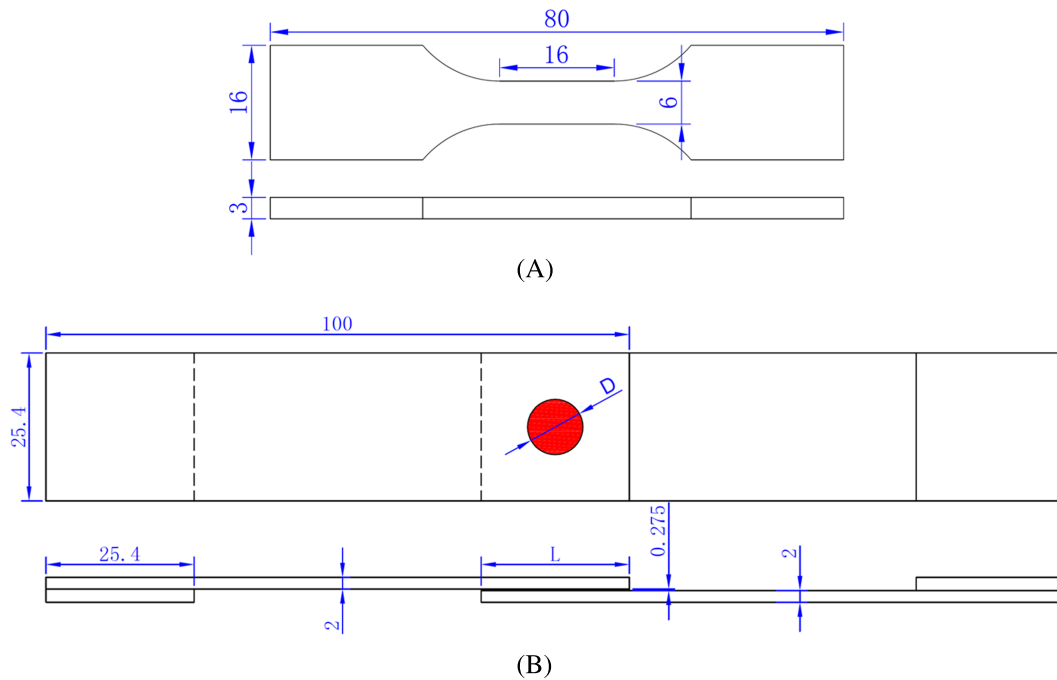
FIGURE 1 (A) Bulk adhesive specimen and (B) adhesive-bonded lap-shear joint configurations and dimensions (unit: mm) [Colour figure can be viewed at wileyonlinelibrary.com]

(round shaded area) for the lap-shear joints. In order to study the effects of different geometric features, six types of lap-shear joints were produced with two types of adhesive fillets, three overlap lengths and two tape diameters. Details of the joints are listed in Table 1. Figure 2 shows the geometries of the arc and full triangular fillets. The detailed dimensions will be shown later in Section 2.2. The mechanical properties of the substrate and the cured adhesive are listed in Table 2. Alcoa 951™ pretreatment was adopted for AA6111-T4 to promote long-term corrosion resistance of the adhesive bond. The thickness of the adhesive layer in the joints was controlled by embedding 0.275-mm diameter glass beads. As suggested by the supplier, the adhesive curing process was performed in an oven at 180°C for 30 min.

All tests were conducted on an MTS servo-hydraulic testing machine under ambient laboratory conditions (room temperature and atmospheric pressure), as shown in Figure 3. A clear plastic cover was used around the testing machine for protection. To eliminate the influence of mean stress, bulk adhesive specimens were tested

under sinusoidal strain-controlled condition at a strain rate of 0.02/s and strain ratio $R = -1$. The extensometer gauge length is 12 mm. The glue was applied at the knife edges of the extensometer to prevent slipping. As for the lap-shear joints, both tensile shear strength and fatigue performance were evaluated. A displacement rate of 3 mm/min was adopted for the tensile tests. Fatigue tests were performed under load-controlled conditions at $R = 0.1$. Constant sinusoidal waveforms at a frequency of 20 Hz were employed for all joints. The specimens were tested to failure or a maximum life of 15 000 000 cycles. The fatigue cycles were determined until the complete separation of joints.

2.2 | Lap-shear joints test results

To illuminate the effects of the adhesive fillet, overlap length and unbonded area, test data are presented against both applied load and tensile shear stress[28] (i.e., maximum tensile load divided by the overlap

TABLE 1 Adhesive-bonded lap-shear joint types

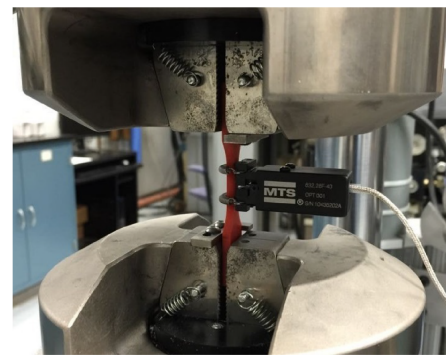| Joints	Type A	Type B	Type C	Type D	Type E	Type F
Bond line length, L (mm)	5.0	12.7	25.4	25.4	25.4	12.7
Tape diameter, D (mm)	0	0	0	8.0	20.0	0
Fillet	Arc	Arc	Arc	Arc	Arc	Full triangular
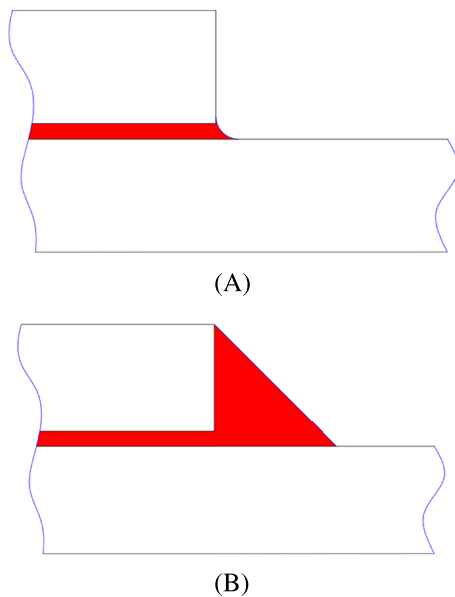
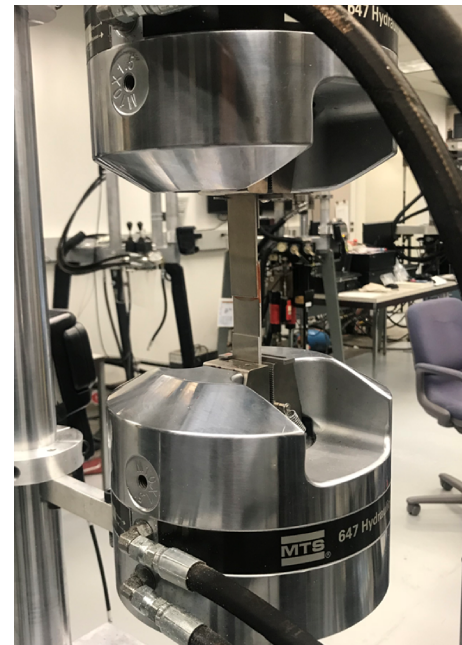**FIGURE 2** Schematics of (A) arc and (B) full triangular fillets [Colour figure can be viewed at wileyonlinelibrary.com]

TABLE 2 Mechanical properties of substrate and adhesive

Materials	Young's Modulus (MPa)	Poisson's ratio	Yield strength (MPa)
AA6111-T4 (substrate)	70 000	0.33	224
BETAMATE 4601™ (adhesive)	2 860	0.35	45

FIGURE 3 Setup of the tests on (A) bulk adhesive specimen and (B) adhesive-bonded lap-shear joint [Colour figure can be viewed at wileyonlinelibrary.com]

area). The comparison of the tensile shear strengths and critical tensile shear stresses between all six types of joints is shown in Figure 4. The influences of the adhesive fillet, overlap length and unbonded area on fatigue failure life are illustrated in Figure 5. In terms of applied load, both the fillet and the overlap length have a positive influence on tensile shear strength and fatigue failure life of adhesive-bonded joints although the mechanisms differ. Furthermore, even with a similar bonded area, for example, a 322.6 mm^2 for Type B and 331.0 mm^2 for Type E, the average tensile shear strength of Type B joint is still much lower than that of Type E joint, which indicates that the actual bonded area is not a quantifying indicator for the strength evaluation of adhesive-bonded joints under lap-shear loading condition. As for tensile shear stress, the effects of the unbonded area and adhesive fillet can be found similar to those for applied load, but the overlap length works oppositely. One of the possible reasons is that although the tensile shear strength of the joints

increases, the actual load-bearing area does not increase proportionally with the overlap area increasing, leading to the decrease of its proportion in the overlap area, and thus the critical tensile shear stress is lowered, and fatigue failure life shortened.

Figure 6 shows the typical fatigue crack path around the adhesive fillets and the dimensions of the local structure. As for an arc fillet, the crack initiation is at the outer edge of the fillet (red arrow shown in Figure 6A), consistent with the observation of Quaresimin and Ricotta.[37] For a full triangular fillet, the corner of the substrate (red arrow shown in Figure 6B) is considered as the crack initiation site based on the simulation results of
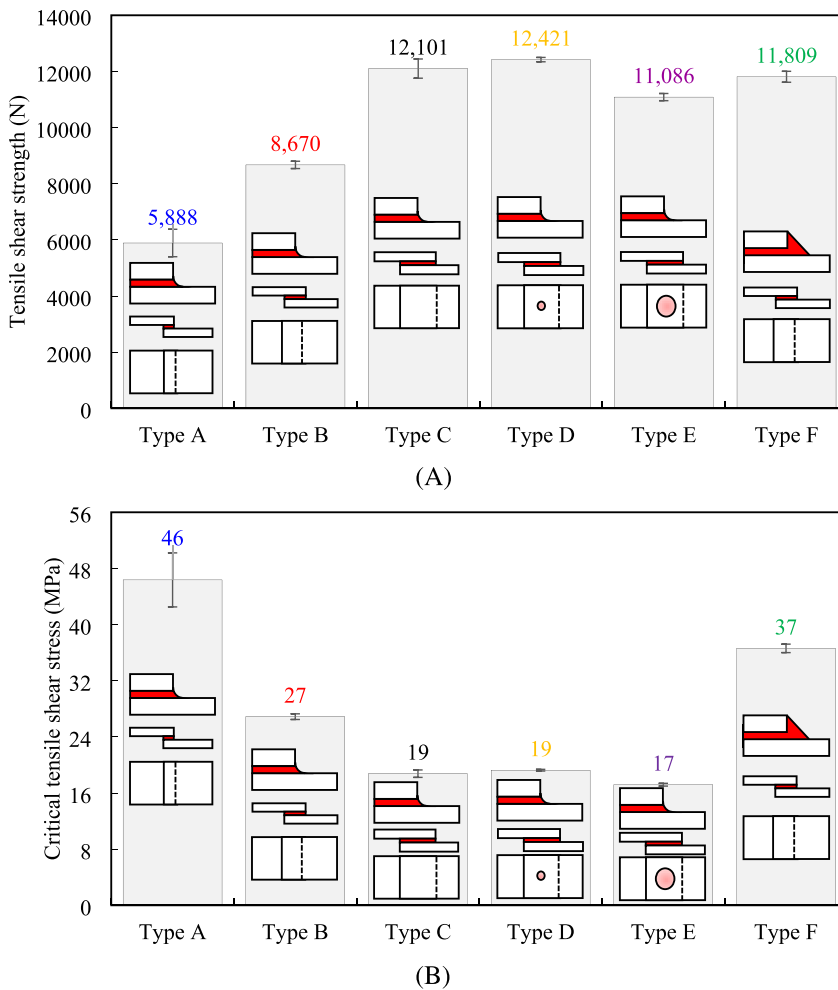
FIGURE 4 Comparison of (A) tensile shear strength and (B) critical tensile shear stress between lap-shear joints [Colour figure can be viewed at wileyonlinelibrary.com]

O'Mahoney et al.[38] and the experimental results of Shenoy et al.[39]

3 | TOTAL FATIGUE LIFE EVALUATION

The total fatigue life of adhesive-bonded joint is calculated by adding the crack initiation life and crack growth life. Initiation life is calculated through a Manson-Coffin-Basquin equation which is fitted by using fatigue test data of bulk adhesive specimens. Detailed FE models of adhesive fillets are adopted to obtain the local strain in order to use this equation for initiation life calculation. Crack growth life is calculated by the integration of loading cycles on the crack growth path. Different crack growth paths are identified for different types of joints.

3.1 | Crack initiation

The local strain-stress approach is adopted to estimate the fatigue failure location and crack initiation lives

based on the widely used assumption[40] that life spent on crack nucleation of a notched component is identical to that of a smooth laboratory specimen under the same cyclic deformation.

3.1.1 | Manson-Coffin-Basquin equation

To correlate the local strain to crack initiation, the strain-life curve of bulk adhesive specimens is described by the classic Manson-Coffin-Basquin equation, as listed in Equation 1, shown in Figure 7 together with the test results.

$$\varepsilon_a = \frac{\sigma'_f}{E}(2N_i)^b + \varepsilon'_f(2N_i)^c, \qquad (1)$$

where ε_a is the strain amplitude, σ'_f and ε'_f, respectively, refer to the fatigue strength coefficient and fatigue ductile coefficient and superscripts b and c are the fatigue strength exponent and the fatigue ductile exponent. All the parameters shown in Equation 1 were obtained through curve fitting and are listed in Table 3.
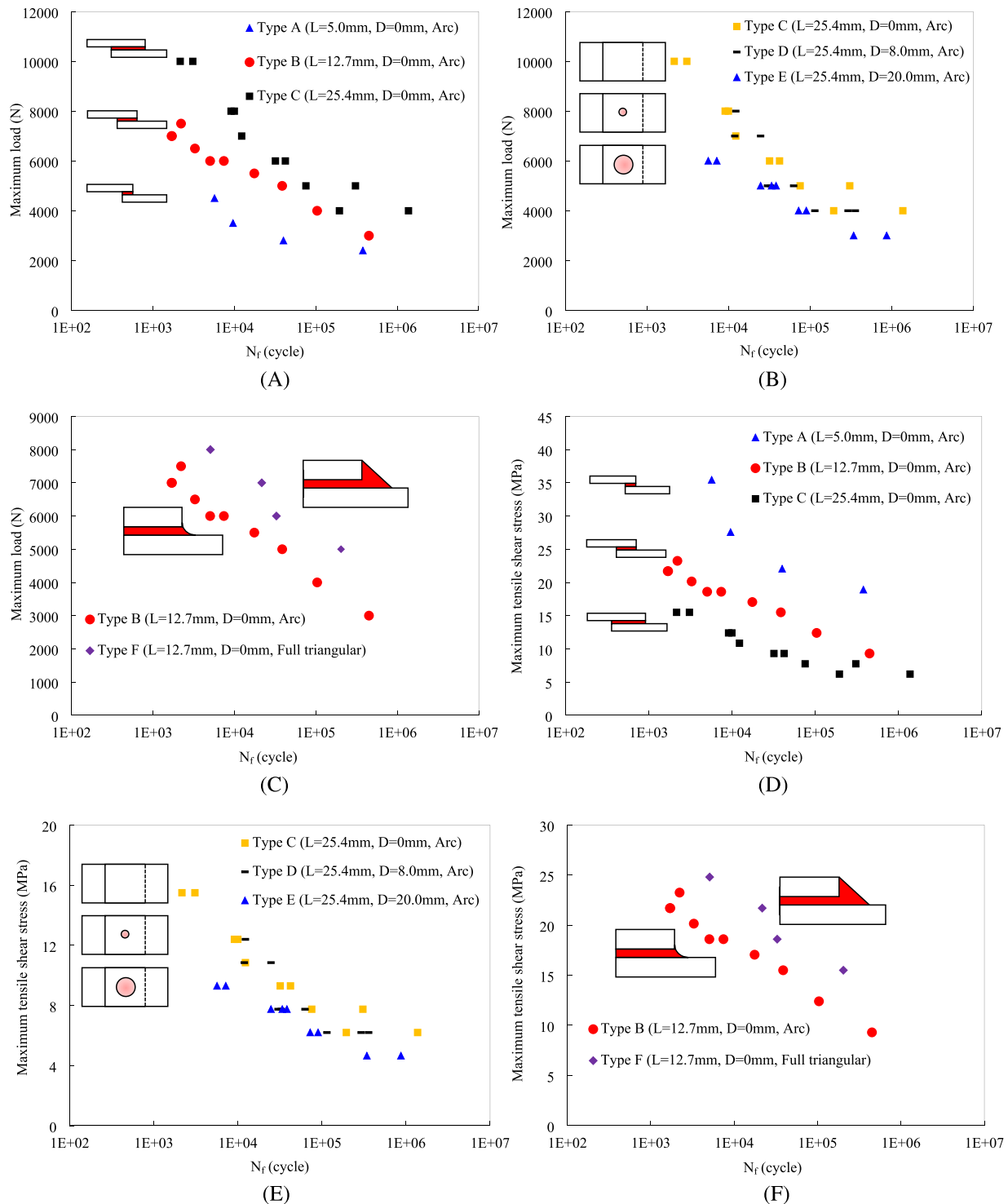
FIGURE 5 Comparison of fatigue failure lives between lap-shear joints on the effects of (A) overlap length, (B) unbonded area, (C) adhesive fillet against applied load and the effects of (D) overlap length, (E) unbonded area, (F) adhesive fillet against tensile shear stress [Colour figure can be viewed at wileyonlinelibrary.com]

3.1.2 | FE models

Full 3D FE models are established by using ABAQUS™/ standard to calculate the local maximum principal strain. Figure 8A,B shows the overviews of typical FE models
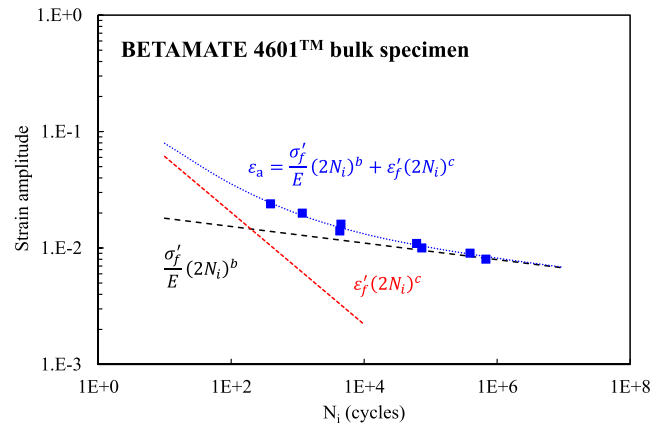
of adhesive-bonded lap-shear joints with arc and full triangular fillets, respectively. An example of the unbonded area in the models is shown in Figure 8C. Models were constructed with 20-node hex elements (C3D20) and refined at adhesive fillets with the element

size of 5 μm, as shown in Figure 8D,E. Figure 9 shows the uniaxial stress-strain curves of the substrate and adhesive used in the FE models.

Figure 10 shows the typical distributions of the maximum principal plastic strain on a symmetric plane in adhesive fillets at an external load of 4000 N. As can be seen from the figures, the crack initiation occurs on the outward side of the fillet in an arc adhesive fillet and at the corner of the substrate for a full triangular adhesive fillet, consistent with experimental results shown in Figure 6. The maximum local principal strain at the crack initiation site will be used to calculate the initiation life through Equation 1 and the calculated results will be presented in Section 4.
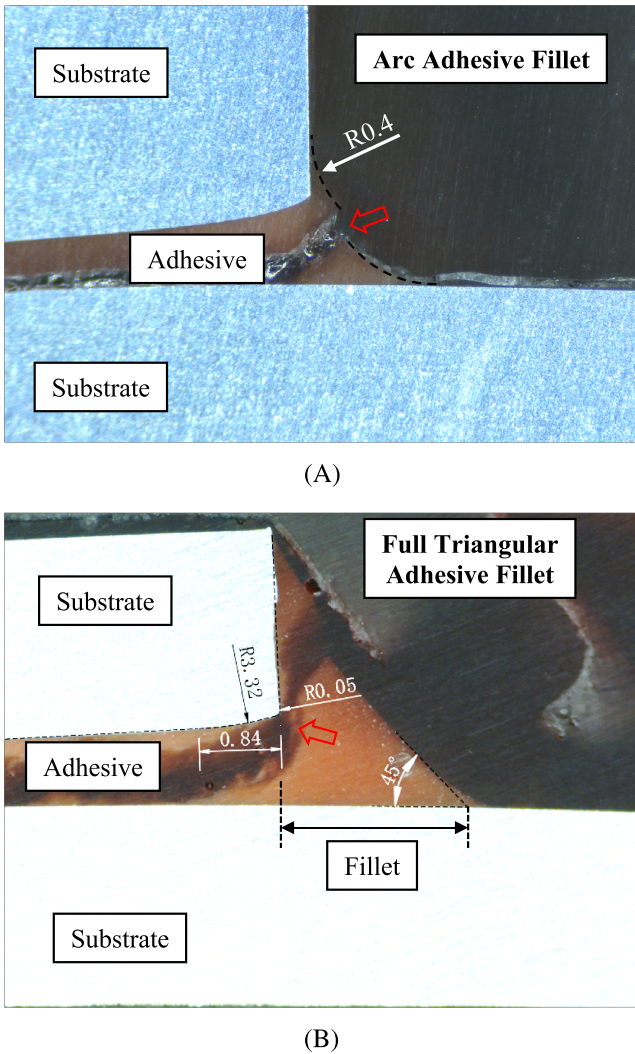
FIGURE 7 Strain-life curve of bulk adhesive specimens [Colour figure can be viewed at wileyonlinelibrary.com]

3.2 | Mixed mode crack growth

Crack growth life is calculated by integrating crack growth rate equation in the form of strain energy release rates from initial crack length to final failure. To account for the mixed mode ratio effect, the interfacial crack model is incorporated into mixed mode crack growth to calculate the strain energy release rate for each mode.

3.2.1 | Strain energy release rates

For simplification, the adhesive layer thickness is neglected due to the small ratio (6%) of bond line thickness to total stack-up thickness. Considering the significant effect of the mixed mode ratio on crack growth rates in an adhesive-bonded system,[30] the interfacial crack model[42,43] is employed to calculate the strain energy release rates for each mode. The schematic of the interfacial crack model is shown in Figure 11. The x-axis is defined to be along the direction from the centre of the adhesive element perpendicularly to the edge of the adhesive layer, the y-axis follows the right-hand rule in $z \times x$, and z is the direction from the thicker substrate to the thinner one. t_l is the thickness of the substrates. F_l and M_l are the line force and line moment applied on the lth layer substrate in FE models (Figure 8), calculated through the structural load method.[3] $l = 1, 2$ for the upper and lower debonded substrates, respectively, and $l = 3$ for the joined side. Assume $t_1 \le t_2$, without loss of generality.

(A)

(B)

FIGURE 6 Fatigue crack path and local structure dimensions in (A) arc and (B) full triangular adhesive fillets (unit: mm; red arrows indicate the fatigue crack initiation sites) [Colour figure can be viewed at wileyonlinelibrary.com]

TABLE 3 Fatigue parameters in the Manson-Coffin-Basquin equation

σ'_f (MPa)	ε'_f (MPa)	b	c	E (MPa)
63.807	0.25819	−0.07118	−0.48082	2860

FIGURE 8 (A) Overview of finite element (FE) model with arc adhesive fillet, (B) overview of FE model with full triangular adhesive fillet, (C) unbonded area in FE model, (D) local mesh in arc adhesive fillet and (E) local mesh in full triangular adhesive fillet [Colour figure can be viewed at wileyonlinelibrary.com]

Unbonded area

(A)

(C)

(D)

(B)

(F)
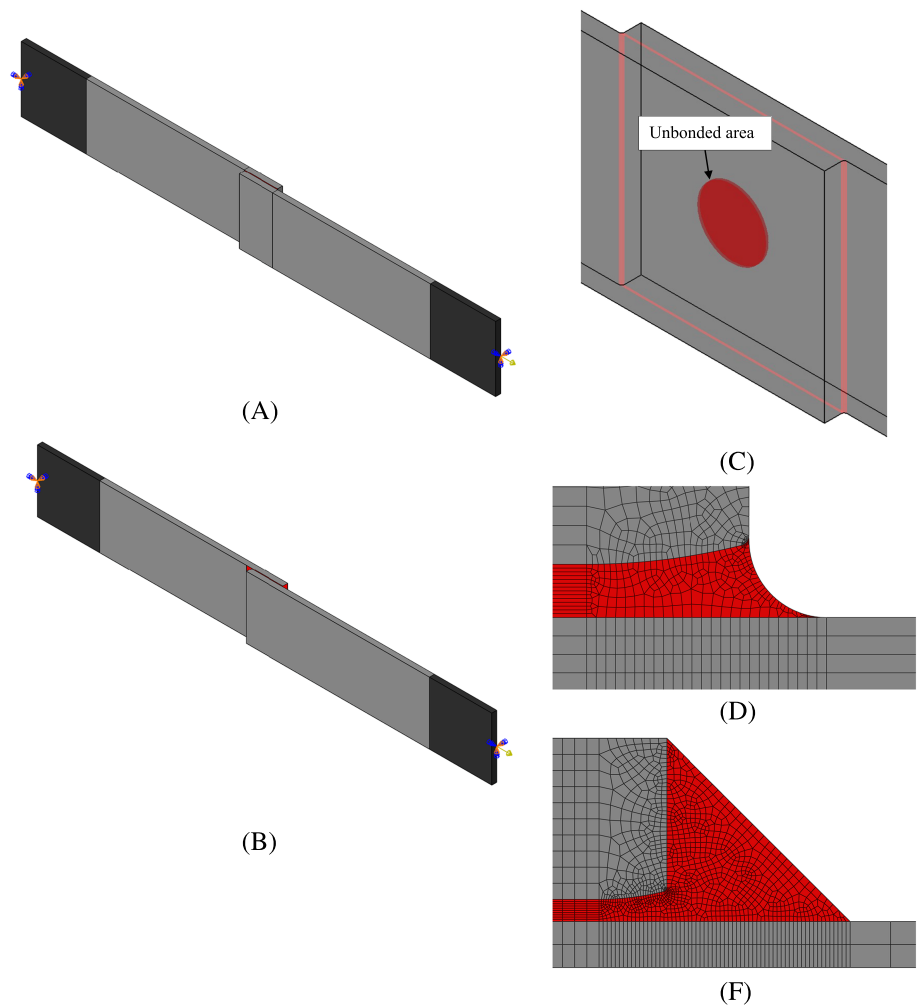
The structural loads that govern the crack tip singularity in Figure 11 can be calculated by superposition methods[42,43] and are as follows:
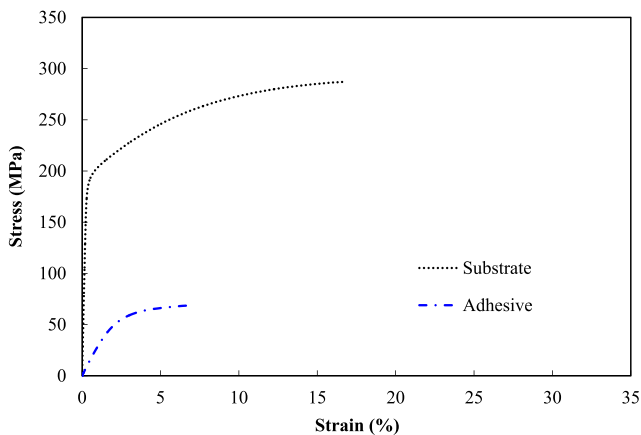
$$F = \frac{1-\eta+\eta^2}{(1+\eta)^3}F_1 - \frac{(1-\eta+\eta^2)\eta}{(1+\eta)^3}F_2 - \frac{6\eta^2}{(1+\eta)^3}(M_1+M_2)/t_1,$$

(2)

$$M = \frac{1+3\eta+3\eta^2}{(1+\eta)^3}M_1 - \frac{\eta^3}{(1+\eta)^3}M_2 - \frac{\eta^3}{2(1+\eta)^3}F_1t_2 + \frac{\eta^3}{2(1+\eta)^3}F_2t_1.$$

(3)

Stress intensity factors (SIFs) for the interfacial crack model in Figure 11 were derived from Hutchinson and Suo and Suo[42,43] numerically by using the structural loads, and expressed as
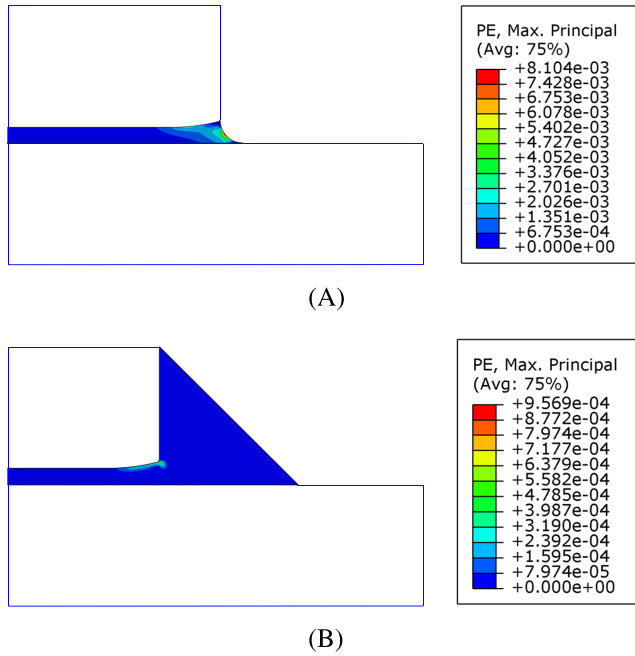
$$K_{\mathrm{I}} = -\left[F\sqrt{\frac{1+4\eta+6\eta^2+3\eta^3}{2t_1}}\cos\alpha + M\sqrt{\frac{6(1+\eta^3)}{t_1^3}}\sin(\alpha+\gamma)\right],$$

(4)

$$K_{\mathrm{II}} = -\left[F\sqrt{\frac{1+4\eta+6\eta^2+3\eta^3}{2t_1}}\sin\alpha - M\sqrt{\frac{6(1+\eta^3)}{t_1^3}}\cos(\alpha+\gamma)\right],$$
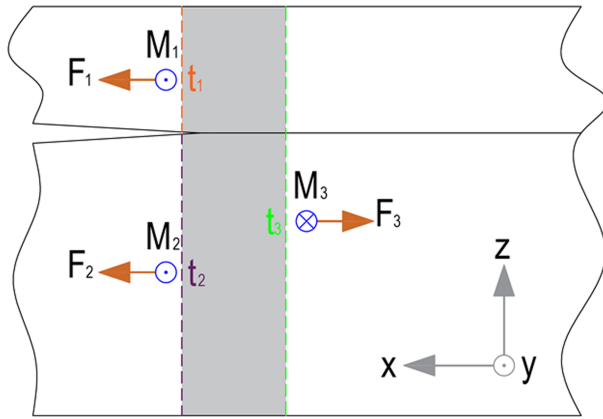
(5)

FIGURE 9 Uniaxial stress-strain curves for substrate and cured adhesive materials (reproduced from Wu et al.[41]) [Colour figure can be viewed at wileyonlinelibrary.com]

FIGURE 10 Distribution of maximum principal plastic strain around adhesive fillets on the symmetric plane in (A) Type B and (B) Type F joints [Colour figure can be viewed at wileyonlinelibrary.com]

FIGURE 11 Schematic of interfacial crack [Colour figure can be viewed at wileyonlinelibrary.com]

where

$$\eta = t_1/t_2, \tag{6}$$

$$\alpha = 52.1° - 3°\eta, \tag{7}$$

$$\sin\gamma = \frac{\sqrt{3}\eta^2(1+\eta)}{\sqrt{(1+4\eta+6\eta^2+3\eta^3)(1+\eta^3)}}. \tag{8}$$

Correspondingly, the strain energy release rates for each mode can be obtained, as follows:

$$G_i = \frac{K_i^2}{E'}, \tag{9}$$

$$E' = \frac{8E_1E_2}{E_2(\kappa_1+1)(\nu_1+1)+E_1(\kappa_2+1)(\nu_2+1)}, \tag{10}$$

$$\kappa_l = \begin{cases} 3-4\nu_l, \text{ for plane strain} \\ \\ \dfrac{3-\nu_l}{1+\nu_l}, \text{ for plane stress} \end{cases}, \tag{11}$$

where K_i (i = I, II) is the ith mode SIF, G_i (i = I, II) is the mode i strain energy release rate calculated using K_i, ν_l and E_l are the Poisson's ratio and Young's modulus at the lth layer, respectively, and E' is the equivalent Young's modulus of the adhesive-bonded structure, substituted by that of the substrate listed in Table 2 for engineering purposes.

3.2.2 | Mixed mode crack growth model

To characterize the mixed mode ratio, the shear mode ratio factor[30] β is calculated as follows and shown in Figure 12 for all kinds of joints.

$$\beta = 1 - \frac{G_I}{G_T}, \tag{12}$$

$$G_T = G_I + G_{II}, \tag{13}$$

where G_I and G_{II} are the mode I and mode II strain energy release rates (N/m) in a loading cycle, respectively. G_T is the corresponding total strain energy release rate.

As can be seen from Figure 12, for the studied lap-shear joints, the mode I strain energy release rate takes about half of the total, and the shear mode ratio factor is uniquely controlled by overlap length. As the overlap length increases from Type A to Type C, the stiffness in overlap area increases and reduces the local bending, leading to a decrease in mode I and an increase in mode II strain energy release rates, which will lower the crack growth rate.[30] On the other hand, the shear mode ratio factor barely changes from Type C to Type E, which may be induced by the unique stress profile in adhesive-

FIGURE 12 Shear mode ratio factor in different joints [Colour figure can be viewed at wileyonlinelibrary.com]
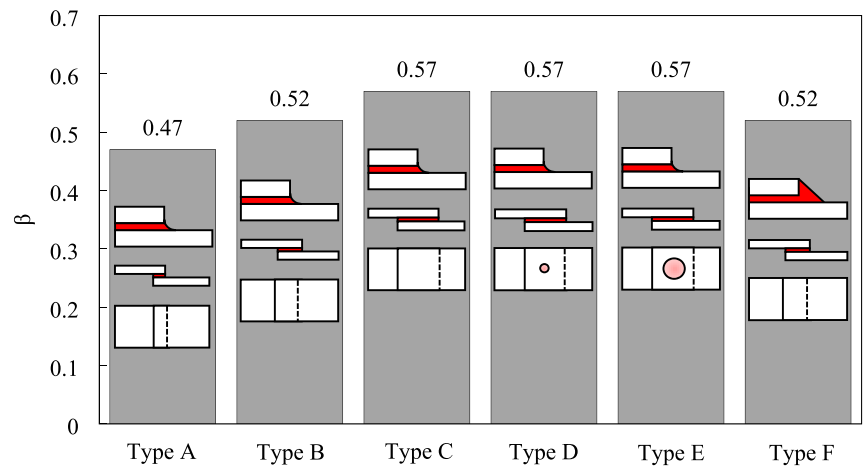
bonded lap-shear joints. Based on the stress analysis in Wu et al,[41] serious stress concentration occurs at the ends of the overlap area in lap-shear joints, and the stress in the central region can be negligible. Most of the applied load in adhesive bonding is carried at the end of the bonded area. The presence of defects in the centre may alter the stress profile in lap-shear joints, but not remarkably, and the load transfer path can hardly be changed, leading to the insignificant variation of structural loads and shear mode ratio factor.

Based on our previous research,[30] the fatigue performance of adhesive-bonded systems is dependent on loading mode mixity. To capture its effect, the mixed mode crack growth rate is expressed by a generalized Paris relation formula[30]:

$$\frac{da}{dN} = c(\beta) \cdot \left(pG_\mathrm{I}^2 + qG_\mathrm{II}^2\right)^{\frac{m(\beta)}{2}}, (\mathrm{mm/cycle}), \quad (14)$$

$$c(\beta) = (1-\beta)c_1 + \beta c_2, \quad (15)$$

$$m(\beta) = (1-\beta)m_1 + \beta m_2, \quad (16)$$

where $c(\beta)$ and $m(\beta)$ are the generalized coefficient and exponent, respectively. p, q, c_1, c_2, m_1 and m_2 are the material constants, which were obtained by fitting the crack growth rate data in our previous work,[30] and listed in Table 4.

The crack growth life can be calculated by integrating the life cycles during crack growth. Based on the simulation results in Chen et al,[30] under shear-dominated loading, the SIFs increase as the crack growing, but not significantly. Thus, the initial strain energy release rates are adopted in the crack growth life calculation of lap-shear joints considering its insignificant variation during the crack evolution. The crack growth life can be derived as

$$N_p = \frac{a_f}{da/dN} \ (\mathrm{cycle}) \quad (17)$$

where a_f is the final crack lengths used for different types of joints. Due to the symmetry, the cracks are treated equally at both loading sides of the studied lap-shear joints. Thus, the final crack lengths are calculated as half of the overlap length for fully bonded joints. For Types D and E joints, the final crack length has to exclude the influence of the unbonded area. Hence, the final crack lengths are counted from the edge of adhesive to the nearest boundary of unbonded area. Table 5 lists the calculated final crack lengths for different types of joints.

TABLE 4 Material constants[30] for fatigue crack growth in BETAMATE 4601™

p	q	c_1	c_2	m_1	m_2
0.1816	0.0583	8.32e-12	1.43e-12	4.14	4.44

TABLE 5 Final crack lengths for different types of joints

| Final crack length	Type A	Type B	Type C	Type D	Type E	Type F
a_f (mm)	2.5	6.35	12.7	8.7	2.7	6.35
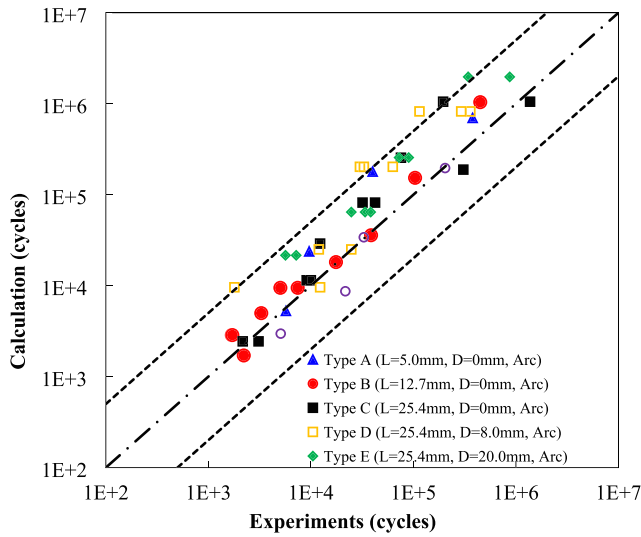
FIGURE 13 Comparison between calculation results and experiments [Colour figure can be viewed at wileyonlinelibrary.com]

4 | RESULTS AND DISCUSSION

Total fatigue failure life is calculated by adding initiation life (in Equation 1) and growth life (in Equation 17). Figure 13 compares the calculated total life with the experimental results. Good correlation between calculation and experimental results is achieved, and most of the data lie within five times of error band.

Figure 14 compares the experimental and calculated results for all types of studied joints by separating the total fatigue life into crack initiation life and growth life. By comparing Figure 14A–C, the crack initiation life is dominant only for the overlap length of 5.0 mm (Type A). As for the overlap length of 12.7 mm (Type B) and 25.4 mm (Type C), the crack growth life is dominant. With the overlap length increasing, the shear mode ratio factor (Figure 12) increases and the fraction of mode II strain energy release rate range (Equation 12) increases, slowing down the crack growth. The increased overlap length also prolongs the growth life by growing length. Figure 14C–E compares the results from Type C to Type E joints. It shows that the unbonded area within the adhesive layer has a similar effect as overlap length. Increasing the unbonded area decreases the crack growth life due to the shorter crack growth length, which explains why fatigue failure life of weld-bonded joints is smaller than that of similar adhesive-bonded joints.[16] However, the initiation life remains similar in three kinds of joints, indicating the insignificant effect of
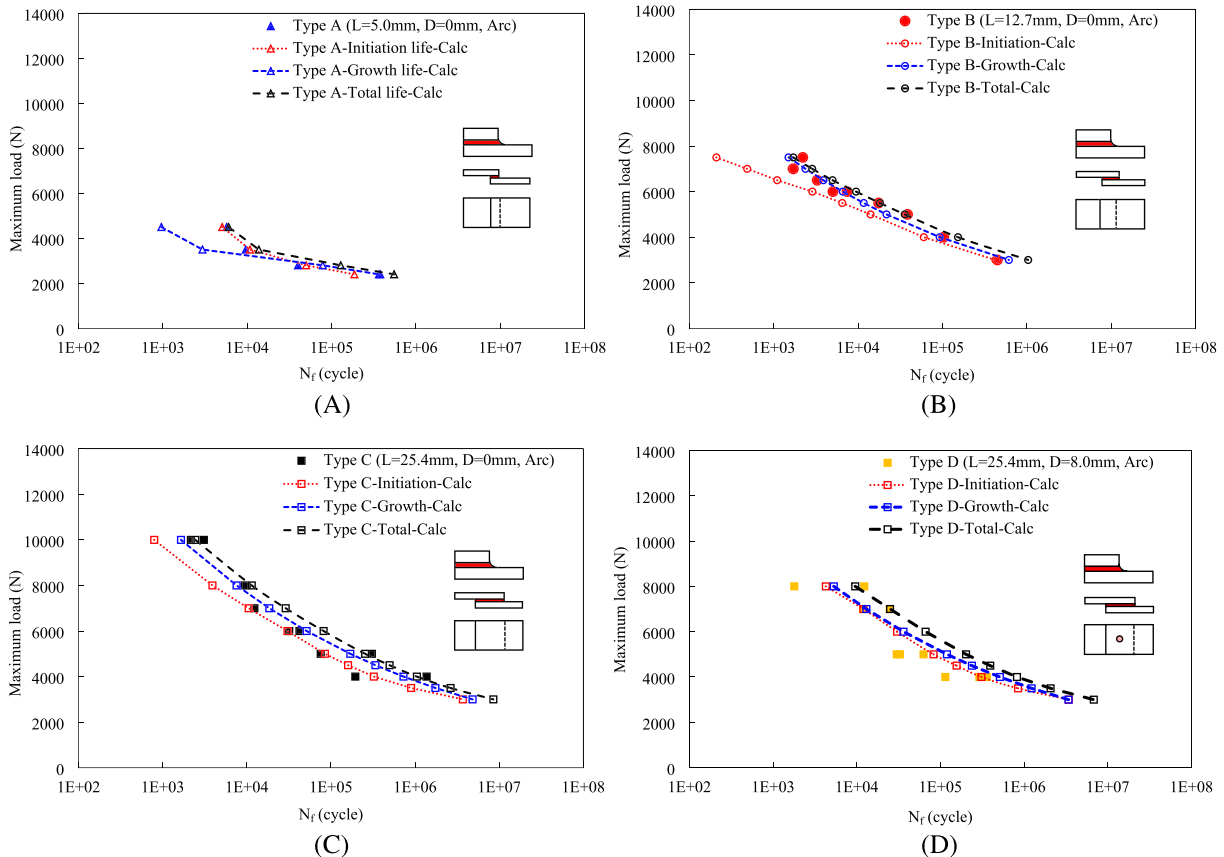
FIGURE 14 Comparison between test results and calculated initiation life, growth life, and the total life in (A) Type A, (B) Type B, (C) Type C, (D) Type D, (E) Type E, and (F) Type F joints [Colour figure can be viewed at wileyonlinelibrary.com]
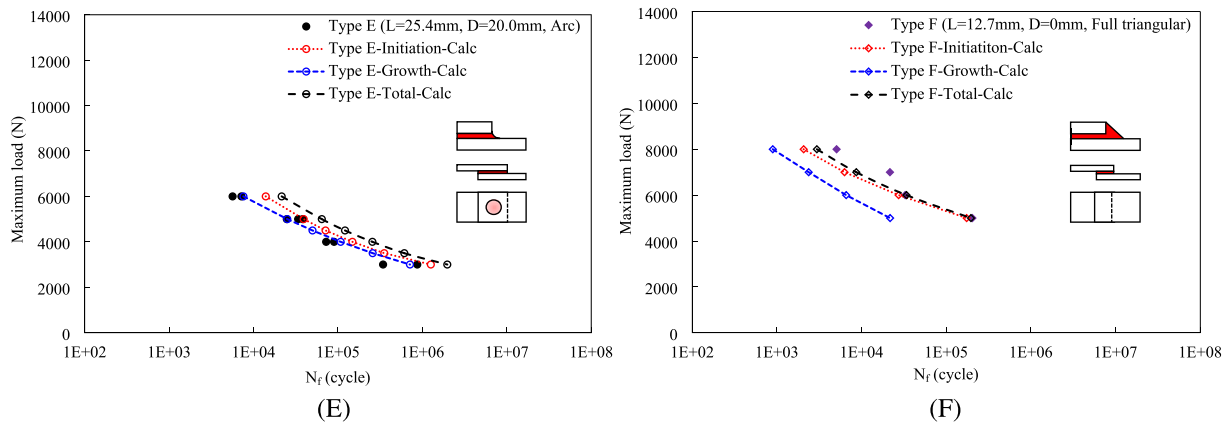
FIGURE 14 (Continued)

unbonded area on crack nucleation. Figure 14B,F compares the results of Type B and Type F joints. It shows that with the same crack growth length and growth life, the full triangular adhesive fillet significantly enhances the crack initiation life, leading to the increasing fatigue failure life of the joints.

5 | CONCLUSIONS

In this work, the effects of the adhesive fillet, overlap length and unbonded area of adhesive-bonded lap-shear joints are experimentally and numerically evaluated. A straightforward total fatigue life calculation method is proposed based on the local strain-stress approach and mixed mode crack growth method. The following conclusions can be drawn:

1. Both the adhesive fillet and the overlap length have a positive influence on the tensile shear strength of adhesive-bonded joints, whereas the unbonded area has a negative impact.
2. By characterizing the initiation life with the local strain-stress approach, the crack initiation life and site are calculated based on detailed FE models. Crack initiation occurs at the outer edge of the arc adhesive fillet and the corner of the substrate edge in a full triangular adhesive fillet.
3. Crack growth life is calculated using the mixed mode crack growth method. An interfacial crack model and a generalized Paris relation formula are utilized to consider the effect of loading mode mixity. Final crack growth length is taken as half of the overlap length for fully bonded joints minus the radius of unbonded area to account for its influence.
4. The entire fatigue failure life of adhesive-bonded joints is calculated by adding up crack initiation and

growth lives. A good correlation between the calculated and the experimental results is obtained.
5. Although both larger adhesive fillet and overlap length enhance the fatigue failure life of adhesive-bonded joints, the mechanisms are completely different. A full triangular adhesive fillet significantly postpones the crack initiation through a lower local strain level. The overlap length increases the crack growth life by enhancing the crack growth length and the fraction of mode II strain energy release rate, which leads to lower crack growth rate.
6. The unbonded area also decreases the crack growth length. Nevertheless, due to the relatively large fraction of the crack initiation life, the effect of the unbonded area on fatigue performance is relatively insignificant.

NOMENCLATURE

E_1, E_2	Young's moduli of upper and lower substrates
F_1, F_2, F_3	line forces applied on upper, lower and joined side substrate

G_1, G_{II}, G_T	mode I, mode II and total strain energy release rates
K_I, K_{II}	mode I and mode II stress intensity factors
M_1, M_2, M_3	line moments applied on upper, lower and joined side substrate
N_i	crack initiation life
N_p	crack growth life
a_F	final crack length
$\frac{da}{dN}$	crack growth rate
t_1, t_2, t_3	upper, lower and joined side substrate thicknesses
ε_a	strain amplitude
ε'_f	fatigue ductile coefficient
v_2, v_2	Poisson's ratios of the upper and lower substrate
σ'_f	fatigue strength coefficient
b	fatigue strength exponent
c	fatigue ductile exponent
D	unbonded area diameter
L	overlap length
E	Young's modulus of the adhesive
E'	Young's modulus of the adhesive-bonded structure
F	structural force that governs the crack tip singularity
M	structural moment that governs the crack tip singularity
$c(\beta)$	generalized coefficient
$m(\beta)$	generalized exponent
p, p, c_1, c_2, m_1, m_2	material constants in generalized Paris relation formula
α, γ	correction angles of stress intensity factors for interfacial crack
β	shear mode ratio factor
η	thickness ratio

ORCID

Dayong Li https://orcid.org/0000-0002-5739-7606
Yandong Shi https://orcid.org/0000-0002-5192-1091

REFERENCES

1. Vantadori S, Camilla R, Carpinteri A. Multiaxial fatigue life evaluation of notched structural components: an analytical approach. *Mater Des Process Commun.* 2019;1(4):e74.
2. Ghosh PK, Avantak P, Kaushal K. Adhesive joining of copper using nano-filler composite adhesive. *Polymer.* 2016;87:159-169.
3. Chen Q, Guo H, Avery K, Su X, Kang H. Fatigue performance and life estimation of automotive adhesive joints using a fracture mechanics approach. *Eng Fract Mech.* 2017;172:73-89.
4. Lißner M, Alabort E, Cui H, Pellegrino A, Petrinic N. On the rate dependent behaviour of epoxy adhesive joints: experimental characterisation and modelling of mode I failure. *Compos Struct.* 2018;189:286-303.
5. De Moura MFSF, Gonçalves JPM, Silva FGA. A new energy based mixed-mode cohesive zone model. *Int J Solid Struct.* 2016;102:112-119.
6. Weißgraeber P, Becker W. Finite fracture mechanics model for mixed mode fracture in adhesive joints. *Int J Solid Struct.* 2013;50(14–15):2383-2394.
7. Han X, Akhmet G, Zhang W, et al. The effect of adhesive fillet on mechanical performance of adhesively bonded corrugated sandwich structures: an experimental–numerical study. *J Adhes.* 2020;96(5):515-537.
8. Zielecki W, Kubit A, Kluz R, Trzepieciński T. Investigating the influence of the chamfer and fillet on the high-cyclic fatigue strength of adhesive joints of steel parts. *J Adhes Sci Technol.* 2017;31(6):627-644.
9. Solana AG, Crocombe AD, Wahab MA, Ashcroft IA. Fatigue initiation in adhesively-bonded single-lap joints. *J Adhes Sci Technol.* 2007;21(14):1343-1357.
10. Abdel Wahab MM. Fatigue in adhesively bonded joints: a review. *ISRN Materials Science*, 2012;2012:1-25.
11. Azari S, Papini M, Schroeder JA, Spelt JK. Fatigue threshold behavior of adhesive joints. *Int J Adhesion Adhesives.* 2010;30(3):145-159.
12. Sugiman S, Crocombe AD. The static and fatigue responses of aged metal laminate doublers joints under tension loading. *J Adhes Sci Technol.* 2016;30(3):313-327.
13. Kumar S, Pandey PC. Fatigue life prediction of adhesively bonded single lap joints. *Int J Adhesion Adhesives.* 2011;31(1):43-47.
14. Miyazaki T, Noda NA. Evaluation of debonding strength of single lap joint by the intensity of singular stress field. Journal of Physics: Conference Series. 2017;842:012078.
15. Pashah S, Arif AFM. Fatigue life prediction of adhesive joint in heat sink using Monte Carlo method. *Int J Adhesion Adhesives.* 2014;50:164-175.
16. Shahani AR, Pourhosseini SM. The effect of adherent thickness on fatigue life of adhesively bonded joints. *Fatigue Fract Eng Mater Struct.* 2019;42(2):561-571.
17. Blaysat B, Hoefnagels JP, Lubineau G, Alfano M, Geers MG. Interface debonding characterization by image correlation integrated with double cantilever beam kinematics. *Int J Solid Struct.* 2015;55:79-91.
18. Kim HB, Naito K, Oguma H. Fatigue crack growth properties of a two-part acrylic-based adhesive in an adhesive bonded joint: double cantilever-beam tests under mode I loading. *Int J Fatigue.* 2017;98:286-295.
19. Al-Khudairi O, Hadavinia H, Waggott A, Lewis E, Little C. Characterising mode I/mode II fatigue delamination growth in unidirectional fibre reinforced polymer laminates. *Mater Des (1980–2015).* 2015;66:93-102.
20. Wahab MA, Ashcroft IA, Crocombe AD, Smith PA. Finite element prediction of fatigue crack propagation lifetime in composite bonded joints. *Compos A: Appl Sci Manuf.* 2004;35(2):213-222.
21. Monteiro J, Akhavan-Safar A, Carbas R, et al. Influence of mode mixity and loading conditions on the fatigue crack

growth behaviour of an epoxy adhesive. *Fatigue Fract Eng Mater Struct*. 2020;43(2):308-316.

22. Ayatollahi MR, Samari M, Razavi SMJ, da Silva LFM. Fatigue performance of adhesively bonded single lap joints with non-flat sinusoid interfaces. *Fatigue Fract Eng Mater Struct*. 2017;40(9):1355-1363.

23. Solana AG, Crocombe AD, Ashcroft IA. Fatigue life and back-face strain predictions in adhesively bonded joints. *Int J Adhesion Adhesives*. 2010;30(1):36-42.

24. Shenoy V, Ashcroft IA, Critchlow GW, Crocombe AD. Unified methodology for the prediction of the fatigue behaviour of adhesively bonded joints. *Int J Fatigue*. 2010;32 (8):1278-1288.

25. Tang JH, Sridhar I, Srikanth N. Static and fatigue failure analysis of adhesively bonded thick composite single lap joints. *Compos Sci Technol*. 2013;86:18-25.

26. Jen YM, Ko CW. Evaluation of fatigue life of adhesively bonded aluminum single-lap joints using interfacial parameters. *Int J Fatigue*. 2010;32(2):330-340.

27. Braga DF, Maciel R, Bergmann L, et al. Fatigue performance of hybrid overlap friction stir welding and adhesive bonding of an Al-Mg-Cu alloy. *Fatigue Fract Eng Mater Struct*. 2019;42(6): 1262-1270.

28. Xu W, Liu L, Zhou Y, Mori H, Chen DL. Tensile and fatigue properties of weld-bonded and adhesive-bonded magnesium alloy joints. *Mater Sci Eng A*. 2013;563:125-132.

29. Abdel Wahab MM, Hilmy I, Ashcroft IA, Crocombe AD. Evaluation of fatigue damage in adhesive bonding: part 2: single lap joint. *J Adhes Sci Technol*. 2010;24(2):325-345.

30. Chen Q, Guo H, Avery K, Kang H, Su X. Mixed-mode fatigue crack growth and life prediction of an automotive adhesive bonding system. *Eng Fract Mech*. 2018;189:439-450.

31. Belnoue JPH, Giannis S, Dawson M, Hallett SR. Cohesive/adhesive failure interaction in ductile adhesive joints part II: quasi-static and fatigue analysis of double lap-joint specimens subjected to through-thickness compressive loading. *Int J Adhesion Adhesives*. 2016;68:369-378.

32. de Moura MFSF, Gonçalves JPM. Cohesive zone model for high-cycle fatigue of composite bonded joints under mixed-mode I+ II loading. *Eng Fract Mech*. 2015;140:31-42.

33. Roe KL, Siegmund T. An irreversible cohesive zone model for interface fatigue crack growth simulation. *Eng Fract Mech*. 2003;70(2):209-232.

34. Khoramishad H, Crocombe AD, Katnam KB, Ashcroft IA. Predicting fatigue damage in adhesively bonded joints using a cohesive zone model. *Int J Fatigue*. 2010;32(7):1146-1158.

35. ISO B. 527–2: 1996. Plastics–determination of tensile properties–part 2: test conditions for moulding and extrusion plastics. British Standards Institution, 1996; 1–14.

36. ASTM. D-3166-99: Standard test method for fatigue properties of adhesives in shear by tension loading (metal/-metal). 2012.

37. Quaresimin M, Ricotta M. Fatigue behaviour and damage evolution of single lap bonded joints in composite material. *Compos Sci Technol*. 2006;66(2):176-187.

38. O'Mahoney DC, Katnam KB, O'Dowd NP, McCarthy CT, Young TM. Taguchi analysis of bonded composite single-lap joints using a combined interface–adhesive damage model. *Int J Adhesion Adhesives*. 2013;40:168-178.

39. Shenoy V, Ashcroft IA, Critchlow GW, Crocombe AD, Wahab MA. An investigation into the crack initiation and propagation behaviour of bonded single-lap joints using back-face strain. *Int J Adhesion Adhesives*. 2009;29(4):361-371.

40. Huang L, Guo H, Shi Y, Huang S, Su X. Fatigue behavior and modeling of self-piercing riveted joints in aluminum alloy 6111. *Int J Fatigue*. 2017;100:274-284.

41. Wu G, Li D, Shi Y, Avery K, Huang L, Huang S, Su X, Peng Y. Stress Analysis on the Single-Lap SPR-Adhesive Hybrid Joint. SAE Technical Paper No. 2018–01–1445, April 2018.

42. Hutchinson JW, Suo Z. Mixed mode cracking in layered materials. *Adv Appl Mech*. 1991;29:63-191.

43. Suo Z. Delamination specimens for orthotropic materials. *J Appl Mech*. 1990;57(3):627-634.